Progress In Electromagnetics Research Letters, Vol. 69, 119–125, 2017

A Compact Quadruple-Mode Ultra-Wideband Bandpass Filter with a Broad Upper Stopband Based on Transversal-Signal Interaction Concepts

Xiuping Li[1, 2, *], Qi Xia[1, 2], and Junjie Zeng[1, 2]

Abstract—In this article, a compact ultra-wideband (UWB) band-pass filter (BPF) with wide upper stopband is presented. The filter is designed with a UWB response from 3.2 GHz to 10.8 GHz with low insertion loss of 0.9 dB and less than 0.19 dB at the center frequency (6.67 GHz). The filter is also designed with a broad upper stopband with high rejection level of 20 dB. The group delay is flat with maximum of 0.4 ns. The proposed UWB filter is constructed by using a pair of parallel coupled lines and two ring resonators. In this design, the ring resonators provide two new excited modes to widen the desired UWB passband and also create two tunable transmission zeros to achieve a wide stopband. Good agreement is observed between simulated and measured performances of the UWB filter.

1. INTRODUCTION

There is an increasing development of UWB technology since the authorization of the unlicensed use of 3.1 to 10.6 GHz for ultra-wideband (UWB) communications by the Federal Communications Commission (FCC) [1]. Much attention has been paid to UWB BPF, serving as a key component in the UWB system, by many researchers. Designing a UWB filter with wide passband, small size, low insertion loss and wide upper stopband is still a challenging task. In recent years, many filters have been developed in various ways. For example, using multiple-mode resonators (MMR) [2–6], using stub-loaded structures [7], using cascaded structures [8–10], and using composite right/left-handed structures [11]. In a previous work [12], a UWB filter is developed by using a pair of coupled lines and two open stubs. The response has a wide upper stopband and good selectivity. However, the bandwidth is not wide enough to satisfy UWB standard. And in another previous work [13], a UWB filter is developed by using two rectangular stub resonators to suppress the spurious passband, replacing the open stubs in [12]. The filter in [13] shows improved result in upper stopband as well as in passband bandwidth.

In this paper, a UWB bandpass filter is designed with high return loss (RL) in the passband and a broad stopband outside of the passband. The response was achieved by using a pair of parallel-coupled line and two ring resonators. The bandstop characteristics of the ring resonator is analyzed based on transversal signal-interaction concepts. It is verified that the ring resonators can not only provide two novel excited modes to improve UWB response but also provide two tunable transmission zeros to form a wide stopband. The result shows that this design is competitive compared with previous works.

2. DESIGN OF THE ULTRA-WIDEBAND BANDPASS FILTER

The geometry of the proposed UWB filter is shown in Figure 1. The filter consists of a pair of parallel-coupled lines and two ring resonators. The filter is fabricated on an Arlon Diclad 800 ^{TM} substrate ($\varepsilon_r = 2.2$, $\delta = 0.0009$, thickness $= 0.787$ mm).

Received 2 January 2017, Accepted 24 May 2017, Scheduled 11 August 2017

* Corresponding author: Xiuping Li (xpli@bupt.edu.cn).

[1] School of Electronic Engineering, Beijing University of Posts and Telecommunications, Beijing 100876, China. [2] Beijing Key Laboratory of Work Safety Intelligent Monitoring, Beijing University of Posts and Telecommunications, Beijing 100876, China.

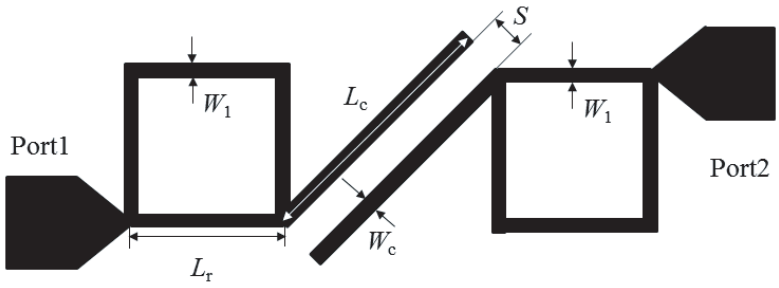

Figure 1. Layout of the proposed UWB BPF. (Dimensions: $L_c = 8\,\text{mm}$, $W_c = 0.1\,\text{mm}$, $S = 0.1\,\text{mm}$, $L_r = 3.4\,\text{mm}$, $W_1 = 0.1\,\text{mm}$, $W_2 = 0.1\,\text{mm}$).

2.1. Design of a Pair of Parallel-Coupled Lines

Figure 2 shows the geometry and response of the parallel-coupled lines. As shown in Figure 2(a), the parallel-coupled lines consist of two parallel microstrip lines with electrical length θ_c and even- and odd-mode characteristic impedances Z_{0o} and Z_{0e}.

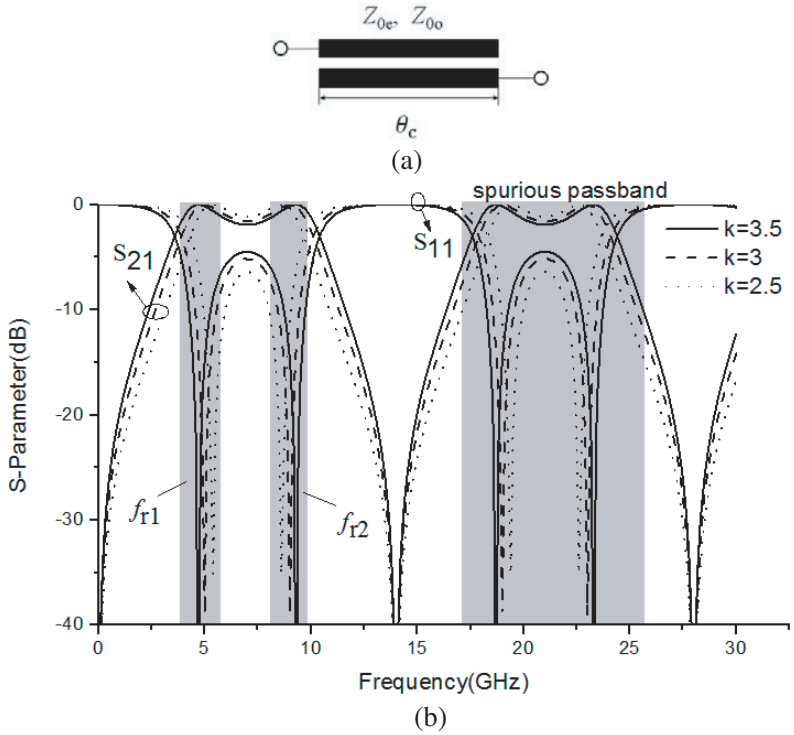

Figure 2. (a) Layout, (b) response of the proposed parallel-coupled lines with different ratio of odd- and even-mode impedances (k) when $Z_{0o} = 83\,\text{Ohm}$ and $L_c = 8\,\text{mm}$.

S_{21} can be expressed in terms of odd- and even-mode impedances Z_{0o} and Z_{0e} as [14]:

$$S_{21} = \frac{2\sin\theta_c}{\left(\dfrac{Z_{0e}+Z_{0o}}{Z_{0e}-Z_{0o}}\right)\left[2\sin\theta_c\cos\theta_c + j\left(\sin^2\theta_c - \cos^2\theta_c\right)\right]} \tag{1}$$

Eq. (1) shows the relationship among Z_{0o}, Z_{0e}, θ_c and S_{21}. The physical length of the parallel-coupled lines (Lc) can be chosen as 8 mm, which is a quarter-wavelength at 6.7 GHz, the center frequency of the desired UWB passband. In addition, an impedance ratio of odd- and even-mode impedances is

defined as $k = Z_{0e}/Z_{0o}$. Figure 2(b) shows the simulated response of the proposed parallel-coupled lines with different ratios of odd- and even-mode impedances (k) when the physical width of the lines is 0.1 mm ($Z_{0o} = 83\,\Omega$hm). It is obvious that there are two resonant frequencies (f_{r1}, f_{r2}) in UWB passband. As k grows, f_{r1} and f_{r2} shift to a lower and higher frequencies, respectively, leading to a wider passband bandwidth. Therefore, to make the passband as wide as possible, the physical width of the gap (S) should be small enough and is determined to be 0.1 mm ($Z_{0e} = 281\,\Omega$hm, $Z_{0o} = 83\,\Omega$hm). Two transmission zeros at 14 GHz and 27.7 GHz are observed. Nevertheless, the structure only provides two modes (f_{r1}, f_{r2}) at 4.9 GHz and 9.3 GHz, respectively, resulting in a narrow passband bandwidth. Moreover, the two resonant frequencies outside the passband result in an unwanted spurious passband with center frequency at 21.3 GHz. Therefore, this structure needs to be improved.

2.2. Design of a Ring Resonator

2.2.1. Design of the Ring Resonators Based on the Stopband Response

In this design, two ring resonators, connected to each side of the parallel-coupled lines, are used to form the upper stopband. The length ratio of the lower part and upper part of the ring resonator is 1 : 3. The geometry of a ring resonator is shown in Figure 3(a). The equivalent circuit of the ring resonator based on transversal signal-interaction concepts is demonstrated in Figure 3(b). The ring resonator has two paths, the upper and lower paths, with characteristic impedance and electrical length at (Z_1, 3θ) and (Z_2, θ), respectively. When $\theta = 90°$, stopband can be achieved because of the phase difference of 180° between the two paths [15]. The stopband performance of the ring resonator can be further analysed by using Y matrix. Its Y matrix can be expressed as:

$$Y = Y_{upper} + Y_{lower} = \begin{bmatrix} -j\left(\dfrac{\cot 3\theta}{Z_1} + \dfrac{\cot\theta}{Z_2}\right) & j\left(\dfrac{1}{Z_1 \sin 3\theta} + \dfrac{1}{Z_2 \sin\theta}\right) \\ j\left(\dfrac{1}{Z_1 \sin 3\theta} + \dfrac{1}{Z_2 \sin\theta}\right) & -j\left(\dfrac{\cot 3\theta}{Z_1} + \dfrac{\cot\theta}{Z_2}\right) \end{bmatrix} \tag{2}$$

where, θ is the electrical length of the lower path.

The relationship between transmission response and Y matrix can be expressed as:

$$S_{21} = \frac{-2Y_{12}Y_0}{\det Y} \tag{3}$$

Therefore, the ring resonator's $|S_{21}|$ can be found:

$$|S_{21}| = \frac{2Y_0\left(\dfrac{1}{Z_1 \sin 3\theta} + \dfrac{1}{Z_2 \sin\theta}\right)}{\det Y} \tag{4}$$

By letting $|S_{21}| = 0$, two transmission zeros are obtained:

$$\theta_{z1} = \arcsin\left(\sqrt{\frac{3Z_1 + Z_2}{4Z_1}}\right) \tag{5}$$

$$\theta_{z2} = \pi - \arcsin\left(\sqrt{\frac{3Z_1 + Z_2}{4Z_1}}\right) \tag{6}$$

where $\theta_{z1} = 2\pi f_{z1} L_r \sqrt{\varepsilon_e}/c$, $\theta_{z2} = 2\pi f_{z2} L_r \sqrt{\varepsilon_e}/c$. ε_e is the effective dielectric constant of the microstrip line, and c is the speed of the light.

Eqs. (5) and (6) show the relationship between the two transmission zeros (f_{z1}, f_{z2}) and characteristic impedances of the two paths Z_1 and Z_2. In this design, the physical width of the lower path (W_2) is chosen as 0.1 mm ($Z_2 = 170\,\Omega$hm), and the physical length of the lower path (L_r) is chosen as 3.4 mm, which is a quarter-wavelength at 18 GHz, the center frequency of the stopband. Based on Eqs. (5) and (6), the positions of f_{z1} and f_{z2}, with different Z_1 when $Z_2 = 170\,\Omega$hm, are demonstrated in Figure 3(c). It can been seen from Eqs. (5), (6) and Figure 3(c) that as the ratio of Z_1/Z_2 increases, f_{z1} and f_{z2} shift to a lower and higher frequencies, respectively. To achieve a wide stopband, the

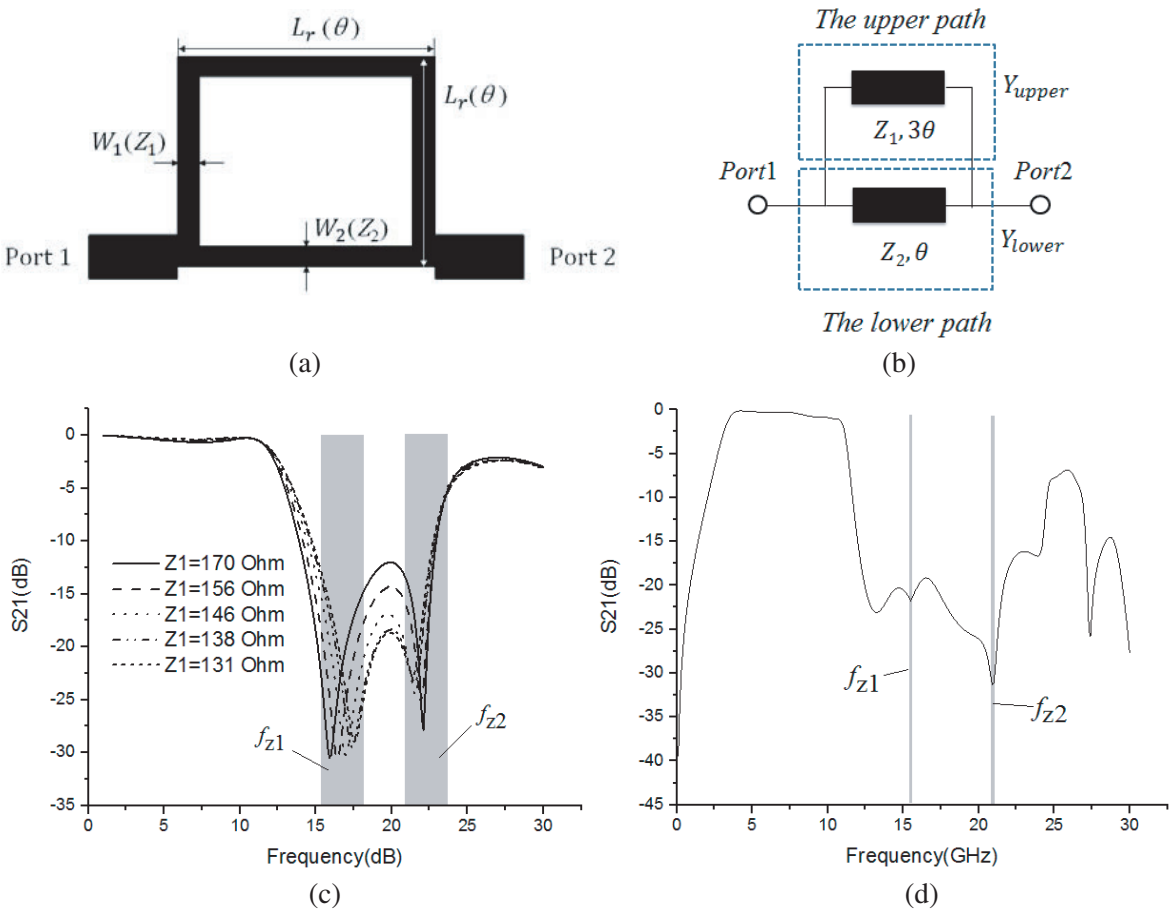

Figure 3. (a) Layout and (b) schematic of the proposed ring resonator. Its lower and upper path have characteristic impedance Z_1 and Z_2, and electrical length 3θ and θ, respectively. (c) The response of the ring resonator with different Z_1 when $Z_2 = 170$, all in Ohm. (d) The response of the UWB filter.

physical width of the upper path is chosen as 0.1 mm ($Z_1 = 170$ Ohm) with a pair of transmission zeros at 15.9 GHz and 22.1 GHz, respectively. Figure 3(d) shows the response of the UWB filter where the two transmission zeros form the stopband.

2.2.2. Analysis of Passband Response

The ring resonators designed in Subsection 2.2.1 can also improve the passband performance. Figure 4 shows the geometry of a ring resonator and its equivalent circuit model. The admittances and electrical lengths of the lower and upper parts of the ring are defined as (Y_1, 2θ) and (Y_2, 6θ), respectively. Thus, the input admittances of odd-mode (Y_{ino}) and even-mode (Y_{ine}) are derived [12]:

$$Y_{ino} = -j\left(\frac{Y_1}{\tan\theta} + \frac{Y_2}{\tan 3\theta}\right) \tag{7}$$

$$Y_{ine} = j\left(Y_1 \tan\theta + Y_2 \tan 3\theta\right) \tag{8}$$

The transfer response can be expressed in terms of Y_{ine} and Y_{ino} [14]:

$$S_{21} = \frac{Y_{ino}}{Y_0 + Y_{ino}} - \frac{Y_{ine}}{Y_0 + Y_{ine}} \tag{9}$$

Obviously, based on Eqs. (7), (8) and (9), when $\mathrm{Im}[Y_{ine}]$ is almost infinite and $\mathrm{Im}[Y_{ino}]$ approximately equal to zero, $|S_{21}|$ is approximately equal to 1, thus an excited mode (f_{r3}) is provided;

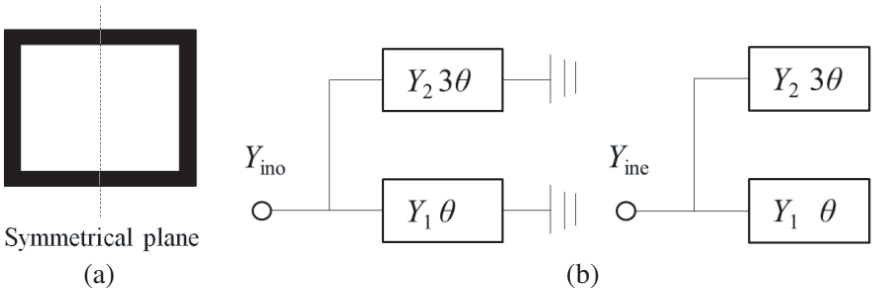

Figure 4. (a) Layout and (b) odd- and even-mode equivalent circuit model of the proposed ring resonator.

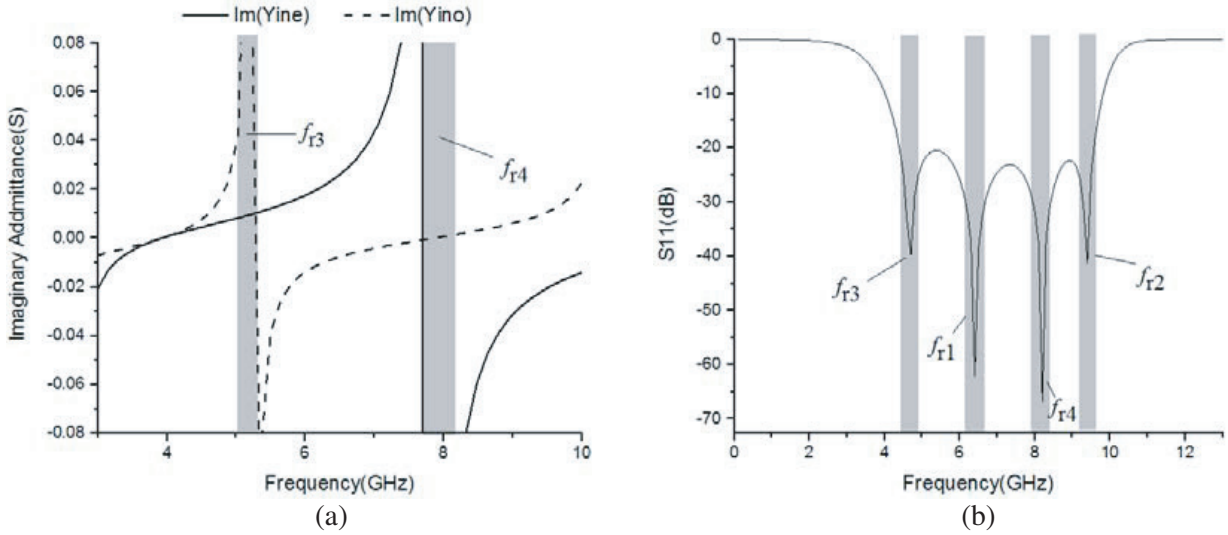

Figure 5. (a) Calculated input admittance of odd- and even-mode (Im[Y_{ino}] and Im[Y_{ine}]). (b) Simulated passband response (S_{11}) of the UWB filter.

when Im[Y_{ino}] is almost infinite and Im[Y_{ine}] approximately equal to zero, $|S_{21}|$ is also approximately equal to 1, thus another excited mode (f_{r4}) is provided. Figure 5 shows how the ring resonators designed in Subsection 2.2.1 provide two new modes in the passband of the UWB filter. The two excited modes therefore are at 4.6 GHz and 8.1 GHz, respectively. In addition, because of the new modes, the original two modes (f_{r1}, f_{r2}) provided by parallel-coupled lines shift to higher frequencies at 6.4 GHz and 9.4 GHz, respectively.

3. RESULTS AND DISCUSSIONS

According to the above analysis and design process, the complete structure shown in Figure 1 is simulated and measured. The UWB BPF is fabricated on a low loss Arlon Diclad 880 substrate ($\varepsilon_r = 2.2$, $\delta = 0.0009$, thickness = 0.787 mm). Figure 6(c) shows the fabricated filter with SMA connectors, and the size of the filter is 12.5 mm × 5 mm.

The filter is measured by Keysight network analyzer. Figure 6(a) shows the comparison of measurement and simulation results. The fabricated UWB filter possesses a fractional bandwidth of 107.7% and broad stopband region up to 24.6 GHz with a high rejection level of 19 dB. The group delay of the measured result shows a small varying range from 0.2 to 0.4 ns. The simulated and measured results agree well. The whole circuit size is about 12.5 mm × 5 mm. Table 1 shows the comparison between this work and the previous works, indicating that this design is competitive.

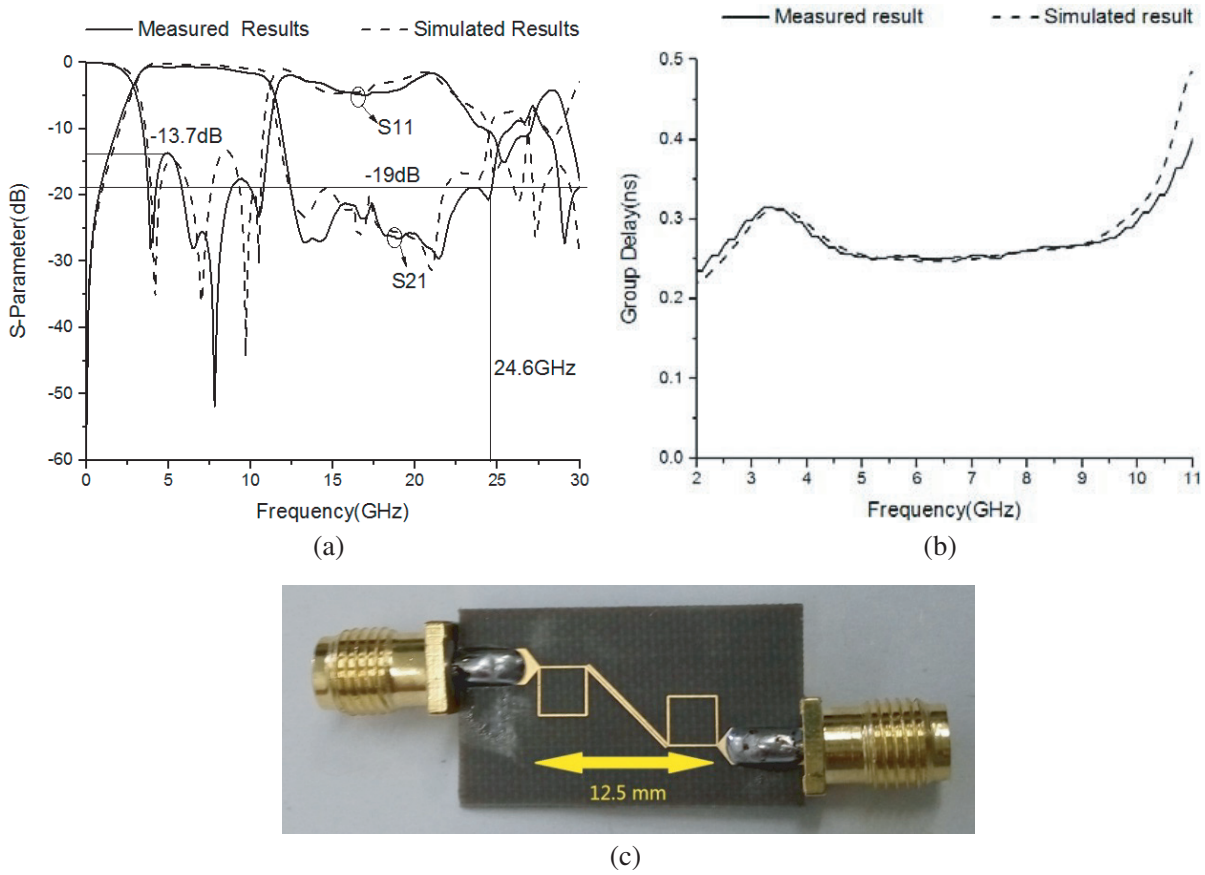

Figure 6. (a) Response and (b) group delay of the simulated and measured results. (c) Photograph of the fabricated UWB filter.

Table 1. Comparison of this work with other references.

Ref.	Size (mm × mm)	FBW(%)	Passband Return Loss (dB)	Stopband (GHz)
[7]	19 × 14	107.7	12	Narrow
[8]	65 × 8	112	> 11	11–20
[9]	10 × 44	98	13	12.6–26.9
[13]	8.1 × 6.1	101.9	14	> 25
This work	12.5 × 5	107.7	> 13.7	> 24.6

4. CONCLUSION

In this paper, a quadruple-mode UWB BPF with a wide passband, high passband return loss and wide upper stopband is presented. A parallel-coupled line structure is analyzed to have a comparatively narrow UWB passband with two resonant modes and an unwanted spurious passband. Then two ring resonators are introduced, which not only provide two new modes to enhance the UWB response, but also create a pair of transmission zeros to form a wide stopband. Transmission zeros are controlled by the impedance of the upper and lower paths of the ring resonators. As shown in Table 1, compared with previous works, the final UWB filter structure has good passband performance, broad stopband region and compact size.

ACKNOWLEDGMENT

This work is supported by the project 61372036 from the National Natural Science Foundation of China (NSFC).

REFERENCES

1. Federal Communications Commission (FCC), "Revision of Part 15 of the Commission's Rules Regarding Ultra-Wideband Transmission Systems," First Report and Order, FCC02. V48, 2002.
2. Chen, H. and Y. X. Zhang, "A novel and compact UWB bandpass filter using microstrip fork-form resonators," *Progress In Electromagnetics Research*, Vol. 77, 273–280, 2007.
3. Peng, H., J. D. Zhao, and B. Wang, "Compact microstrip UWB bandpass filter with triple-notched bands and wide upper stopband," *Progress In Electromagnetics Research*, Vol. 144, 185–191, 2014.
4. Khalid, S., W. P. Wen, and L. Y. Cheong, "A novel synthesis procedure for ultrawideband (UWB) bandpass filters," *Progress In Electromagnetics Research*, Vol. 141, 249–266, 2013.
5. Wong, S. W. and L. Zhu, "Quadruple-mode UWB band-pass filter with improved out-of-band rejection," *IEEE Microwave and Wireless Components Letters*, Vol. 19, No. 3, 152–154, 2009.
6. Zhu, L., S. Sun, and W. Menzel, "Ultra-wideband (UWB) band-pass filters using multiple-mode resonator," *IEEE Microwave and Wireless Components Letters*, Vol. 15, No. 11, 796–798, 2005.
7. Li, X. P. and X. Ji, "Novel compact UWB band-pass filters design with cross-coupling between short-circuited stubs," *IEEE Microwave and Wireless Components Letters*, Vol. 24, No. 1, 2325, 2014.
8. Liu, Y., C. H. Liang, and Y. J. Wang, "Ultra-wideband band-pass filter using hybrid quasi-lumped elements and defected ground structure," *IET Electronics Letters*, Vol. 45, No. 17, 899–900, 2009.
9. Tang, C. W. and M. G. Chen, "A microstrip ultra-wideband band-pass filter with cascaded broadband band-pass and band-stop filters," *IEEE Transactions on Microwave Theory and Techniques*, Vol. 55, No. 11, 2412–2418, 2007.
10. Lee, J. K. and Y. S. Kim, "Ultra-wideband band-pass filter with improved upper stopband performance using defected ground structure," *IEEE Microwave and Wireless Components Letters*, Vol. 20, No. 6, 316–318, 2010.
11. Huang, J.-Q. and Q.-X. Chu, "Compact UWB band-pass filter utilizing modified composite right/left-handed structure with cross coupling," *Progress In Electromagnetics Research*, Vol. 107, 179–186, 2010.
12. Hung, C. Y., M. H. Weng, R. Y. Yang, and Y. K. Su, "Design of the compact parallel coupled wideband bandpass filter with very high selectivity and wide stopband," *IEEE Microwave and Wireless Components Letters*, Vol. 17, No. 7, 510–512, July 2007.
13. Lan, S.-W., M.-H. Weng, C.-Y. Hung, and S.-J. Chang, "Design of a compact ultra-wideband bandpass filter with an extremely broad stopband region," *IEEE Microwave and Wireless Components Letters*, Vol. 26, No. 6, 894–896, June 2016.
14. Zhu, L., S. Sun, and R. Li, *Microwave Bandpass Filters for Wideband Communications*, Wiley, New Jersey, USA, 2001.
15. Feng, W. J., W. Q. Che, and T. F. Eibert, "Ultra-wideband bandpass filter based on transversal signal-interaction concepts," *IET Electronics Letters*, Vol. 47, No. 24, 1330–1331, 2011.